Dynamics and Phase Transitions in Spin-Crossover Complexes: X-ray Structures and Basic Crossover Phenomena in the Solvate Series $[Fe(3\text{-}OEt\text{-}SalAPA)_2](ClO_4)\cdot S$

Andrew J. Conti,[1] Raj K. Chadha,[1] Kathryn M. Sena,[1] Arnold L. Rheingold,*[,2] and David N. Hendrickson*[,1]

Department of Chemistry-0506, University of California at San Diego, La Jolla, California 92093-0506, and Department of Chemistry, University of Delaware, Newark, Delaware 19716

Received July 22, 1992

X-ray structural, ^{57}Fe Mössbauer, X-band EPR, and magnetic susceptibility data are presented for the series of spin-crossover complexes $[Fe(3\text{-}OEt\text{-}SalAPA)_2](CLO_4)\cdot S$, where the solvate molecule S is either absent or is C_6H_6, C_6H_5Cl, C_6H_5Br, or $o\text{-}C_6H_4Cl_2$ and the ligand 3-OEt-SalAPA$^-$ is the Schiff base condensed from 1 mol of 3-ethoxysalicylaldehyde with *N*-aminopropylaziridine. $[Fe(3\text{-}OEt\text{-}SalAPA)_2](ClO_4)\cdot C_6H_5Cl$ crystallizes in the monoclinic space $P2_1/c$ which at 296 K has $a = 13.834(4)$ Å, $b = 17.706(5)$ Å, $c = 15.767(3)$ Å, $\beta = 110.11(2)°$, and $Z = 4$; $R = 0.072$ and $R_w = 0.075$. At 158 K this same C_6H_5Cl solvate crystallizes in the monoclinic space group $P2_1/a$ with $a = 13.604(12)$ Å, $b = 17.475(13)$ Å, $c = 15.379(12)$ Å, $\beta = 109.24(7)°$, and $Z = 4$; $R = 0.049$ and $R_w = 0.052$. In converting from $P2_1/c$ at 296 K to $P2_1/a$ at 158 K the cations and anions of $[Fe(3\text{-}OEt\text{-}SalAPA)_2](ClO_4)\cdot C_6H_5Cl$ remain in the same relative positions, however half of the C_6H_5Cl solvate molecules experience a reorientation. $[Fe(3\text{-}OEt\text{-}SalAPA)_2](ClO_4)\cdot C_6H_5Br$ makes the same phase transition. At 296 K this C_6H_5Br solvate crystallizes in the monoclinic space group $P2_1/c$ with $a = 13.860(4)$ Å, $b = 17.810(5)$ Å, $c = 15.843(3)$ Å, $\beta = 110.10(2)°$, and $Z = 4$; $R = 0.088$ and $R_w = 0.090$. At 163 K the C_6H_5Br solvate is found to be in the monoclinic space group $P2_1/a$ with $a = 13.666(4)$ Å, $b = 17.554(5)$ Å, $c = 15.537(4)$ Å, $\beta = 109.20(2)°$, and $Z = 4$; $R = 0.069$ and $R_w = 0.097$. $[Fe(3\text{-}OEt\text{-}SalAPA)_2](ClO_4)\cdot o\text{-}C_6H_4Cl_2$ crystallizes in the monoclinic space group $C2/c$, which at 298 K has $a = 17.187(8)$ Å, $b = 17.807(7)$ Å, $c = 13.899(8)$ Å, $\beta = 119.94(4)°$, and $Z = 4$; $R = 0.055$ and $R = 0.076$. From powder XRD data it is found that the nonsolvated $[Fe(3\text{-}OEt\text{-}SalAPA)_2](ClO_4)$ is isostructural to $[Fe(3\text{-}OMe\text{-}SalAPA)_2](ClO_4)$, which has been reported to crystallize in the triclinic space group $P\bar{1}$ ($Z = 2$) at 295 K. In the series there are at least five different crystallographic phases. Variable-temperature ^{57}Fe Mössbauer and EPR data show that all complexes in the series are converting from low spin at low temperatures to high spin at high temperatures. Mössbauer spectra run for different preparations of a given complex show that there is a sample history dependence where in some samples the complexes are interconverting between low- and high-spin forms at a rate faster than the ^{57}Fe Mössbauer time scale and an average signal is seen. For other samples separate signals can be seen for low- and high-spin complexes. From the magnetic susceptibility data it is found that the nonsolvated complex changes most gradually (*i.e.*, large temperature range for complete transformation). The C_6H_5Cl solvate makes the most abrupt transformation.

Introduction

Transition-metal complexes which exhibit the spin-crossover phenomenon have received much attention in the past several years.[3] A spin-crossover complex has two electronic states (low- and high-spin) in close energy proximity. This leads to vibronic interactions[4] and, consequently, spin-crossover complexes are appreciably responsive to environmental factors. There are at least three general reasons why these complexes are being studied. First, spin state changes can be rate determining in several biological systems. The biological importance of the spin-crossover phenomenon has been discussed.[5,6] The second general reason for studying spin-crossover complexes relates to the fundamental issue of what controls a spin-state change for an isolated molecule. The kinetically controlled reluctance of triplet O_2 to react with singlet organic molecules is well documented.[7] Metal sites in enzymes catalyze reactions of O_2 with organic substrates by helping overcome the spin forbiddenness. The rate at which an organic molecule can interconvert between singlet and triplet states is *relatively* slow. On the other hand, several Fe^{III} spin-crossover complexes are known,[3a] which interconvert between $^2T_2$ and $^6A_1$ states at a rate greater than $\sim 10^9$ s^{-1} at room temperature. Clearly the increased spin–orbit interaction present in the metal complex is influential in establishing a faster rate of spin-state interconversion in a metal complex than is present for organic molecules. The laser flash-photolysis technique has been used to measure directly the spin-state interconversion rate

(1) University of California at San Diego.
(2) University of Delaware.
(3) (a) Beattie, J. K. *Adv. Inorg. Chem.* **1988**, *32*, 1–53. (b) König, E. *Prog. Inorg. Chem.* **1987**, *35*, 527–622. (c) Rao, C. N. R. *Int. Rev. Phys. Chem.* **1985**, *4*, 19. (d) Gütlich, P. *Struct. Bonding (Berlin)* **1981**, *44*, 83. (e) Goodwin, H. A. *Coord. Chem. Rev.* **1976**, *18*, 293. (f) Scheidt, W. R.; Reed C. A. *Chev. Rem.* **1981**, *81*, 543. (g) König, E.; Ritter, G.; Kulshreshtha, S. K. *Chem. Rev.* **1985**, *85*, 219. (h) Bacci, M. *Coord. Chem. Rev.* **1988**, *86*, 245. (i) Gütlich, P. In *Chemical Mössbauer Spectroscopy*; Herber, R. H. Ed.; Plenum Press: New York, 1984. (j) Maeda, Y.; Takashima, Y. *Comments Inorg. Chem.* **1988**, *7*, 41. (k) Gütlich, P.; Hauser, A. *Coord. Chem. Rev.* **1990**, *97*, 1–22.
(4) (a) Bersuker, I. B.; Polinger, V. Z. *Vibronic Interactions in Molecules and Crystals*; Springer-Verlag: Berlin, 1989. (b) Kambara, T. *J. Chem. Phys.* **1981**, *74*, 4557.
(5) (a) Maltempo, M. M.; Moss, T. H. *Q. Rev. Biophys.* **1976**, *9*, 81. (b) Emptage, M. H.; Zimmerman, R.; Que, L., Jr.; Münck, E.; Hamilton, W. d.; Orme-Johnson, W. H. *Biochim. Biophys. Acta* **1977**, *495*, 12. (c) Messana, C.; Cerdonio, M.; Shenkin, P.; Noble, R. W.; Fermi, G.; Perutz, R. N.; Perutz, M. F. *Biochemistry* **1978**, *17*, 3653. (d) Champion, P. M.; Münck, E.; Debrunner, P. G.; Hollenberg, P. F.; Hager, L. P. *Biochemistry* **1973**, *12*, 426. (e) Dyson, H. J.; Beattie, J. K. *J. Biol. Chem.* **1982**, *257*, 2267. (f) Fisher, M. T.; Sligar, S. G. *Biochemistry* **1987**, *26*, 4797–4803.
(6) (a) Backes, W. L.; Sligar, S. G.; Schenkman, J. B. *Biochemistry* **1982**, *21*, 1324–1330. (b) Tamburini, P. P.; Gibson, G. G.; Backes, W. L.; Sligar, S. G.; Schenkman, J. B. *Biochemistry* **1984**, *23*, 4526–4533.
(7) (a) Hamilton, G. A. Chemical Models and Mechanisms for Oxygenases. In Molecular Mechanisms of Oxygen Activation; Hayaishi, O., Ed.; Academic Press: New York, 1974; pp. 405–451. (b) Taube, H. *J. Gen. Physiol.* **1965**, *49*, 29. (c) Malmström, B. G. *Annu. Rev. Biochem.* **1982**, *51*, 21. (d) Ingraham, L. L.; Meyer, D. L. *Biochemistry of Dioxygen*; Plenum, New York, 1985.

0020-1669/93/1332-2670$04.00/0

in spin-crossover complexes.[8] Very recently this same technique was used for a Fe^{II} spin-crossover complex doped into a polymer film to measure the $^5T_2$ to $^1A_1$ relaxation rate from 300 to 4.2 K.[9] This rate was found to be temperature independent and appreciable ($\sim 10^5$ s^{-1}) in the 4.2–120 K range, which was interpreted as direct evidence of nuclear tunneling as the mechanism of spin-state interconversion. This same type of temperature independence of relaxation rate below ~150 K has been confirmed for several Fe^{II} spin-crossover complexes in two other laboratories.[10]

Understanding the factors which control the spin-crossover transformation in the solid state is the third general reason for studying crossover complexes. Several factors have been found to be important. The introduction of solvate molecules into the lattice,[11] changing the counterion[12] (*e.g.* ClO_4^- to PF_6^-), doping the iron spin-crossover complex into an isostructural host lattice,[13] and even simply mild grinding of the spin-crossover complex[14] have been shown to have a dramatic impact on the spin-crossover transformation in the solid state. The importance of understanding all of the factors which influence a spin-crossover complex in the solid state has increased dramatically with the discovery of the interesting LIESST (light induced excited spin state trapping) effect. Gütlich and co-workers[15,16] first observed the LIESST effect. The observation of the LIESST effect has led to the suggestion[10c,17] that small collections of spin-crossover complexes could be employed as optical memory devices. Laser light at one wavelength could be used to flip the collection of complexes from low to high spin, whereas, laser light of a different wavelength would flop the collection back to the low-spin description.

In the solid state some spin-crossover transformations occur abruptly in a narrow temperature range (<20 deg) and others occur very gradually. In the latter case each complex in the crystal acts independently of its neighbors. There is simply a Boltzmann distribution of complexes in the high- and low-spin states. The benchmark heat capacity paper of Sorai and Seki[18] showed with a sharp heat capacity peak that the abrupt spin-crossover transformation for $Fe(phen)_2(NCS)_2$ occurs in a phase transition. Also, they found that the entropy gain for the phase transition had an appreciable phonon contribution. A small number of spin-crossover complexes are known.[3b-d] which exhibit abrupt spin-crossover transformations. A few of these have been shown with heat capacity data to involve phase transitions.[18,19] There are also a small number of spin-crossover complexes which have gradual enough transformations such that they reflect Boltzmann distributions. There is no cooperativity of spin-state interconversion between complexes in the solid state in this case. However, it appears that for the bulk of spin-crossover complexes that the spin-sate transformation is intermediate between "abrupt" and "gradual".

In this and the following paper an appreciable data base is presented for the series $[Fe(3\text{-}OEt\text{-}SalAPA)_2](ClO_4)\cdot S$, where the tridentate ligand $(3\text{-}OEt\text{-}SalAPA)^-$ is

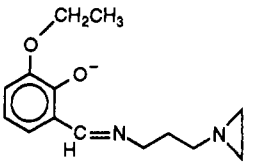

$(3\text{-}OEt\text{-}SalAPA)^-$

and the solvate molecule S is either absent or is C_6H_6, C_6H_5Cl, C_6H_5Br, or $o\text{-}C_6H_4Cl_2$. As the solvate molecule is changed in this series, the level of abruptness of the spin-state transformation does change, as established by magnetic susceptibility data in this first paper. Powder XRD patterns and single-crystal X-ray structures for all of the complexes show that the basic solid-state packing arrangement is the same in the series. There are subtle differences in the disposition of the solvate molecule. **At least five different crystallographic phases (unit cells) are found in the series.** In the second paper heat capacity data are presented for four of the complexes to confirm there are several phase transitions and to give accurate thermodynamic data for the phase transitions. In the second paper an explanation is advanced for the origin of all the different phases. Also, for the first time, solid-state ^2H NMR is used to monitor the onset of dynamics associated with solvate molecules in a spin-crossover complex.

Experimental Section

Sample Preparation. The non-solvated form of $[Fe(3\text{-}OEtSalAPA)_2]ClO_4$ was prepared as reported previously[20] for $[Fe(SalAPA)_2]ClO_4$, except that 3-ethoxysalicylaldehyde was used in place of salicylaldehyde. Two methods of preparation of the solvated complexes were used in this study.

Method I. The solvates of composition $[Fe(3\text{-}OEt\text{-}SalAPA)_2](ClO)_4\cdot S$ were prepared by recrystallizing from 200 to 700 mg of the non-solvated complex in approximately 80 mL of dichloromethane. First the CH_2Cl_2 solution was filtered and then 15–25 mL of the solvate molecule were added to the solution dropwise. Crystallization occurred over a period of 1 day. The crystals were then collected and washed with cold ether.

Method II. A second method was employed to prepare the large samples needed for the heat capacity experiments. In this second method of preparation approximately 18 g of the nonsolvated complex was dissolved in 1.3–1.6 L of dichloromethane and this solution was filtered. To this solution were added dropwise with stirring approximately 0.5 L of the respective solvate. This solution was allowed to remain in an open vessel in a hood where crystallization of the product occurred over a 6-day period.

The chemical analysis data of compounds prepared using either methods agree very well with the theoretical values. The data are available in the supplementary material.

(8) (a) Lawthers, I.; McGarvey, J. I. *J. Am. Chem. soc.* **1984**, *106*, 4280. (b) McGarvey, J. J.; Lawthers, I.; Toftlund, H. *J. Chem. Soc., Chem. Soc., Chem. Commun.* **1984**, 1576. (c) McGarvey, J. J.; Lawthers, I. *Ibid* **1982**, 906. (d) McGarvey, J. J.; Lawthers, I.; Heremans, K.; Toftlund, H. *Inorg. Chem.* **1990**, *29*, 252–256. (e) Conti, A. J.; Xie, C.-L.; Hendrickson, D. N. *J. Am. Chem. Soc.* **1989**, *111*, 1171–1180.

(9) Xie, C.-L.; Hendrickson, D. N. *J. Am. Chem. Soc.* **1987**, *109*, 6981–6988.

(10) (a) Hauser, A.; Gütlich, P. Presented at the Eighth International Symposium on the Photochemistry and Photophysics of Coordination Compounds, August 12–18, 1989, University of California, Santa Barbara. (b) McGarvey, J. J. Private communication. (c) Gütlich, P.; Hauser, A. *Pure Appl. Chem.* **1989**, *61*, 849–854.

(11) (a) Renovitch, G. A.; Baker, A., Jr. *J. Am. Chem. Soc.* **1967**, *89*, 6377. (b) Sorai, M.; Ensling, J.; Hasselbach, K. M.; Gütlich, P. *Chem. Phys.* **1977**, *20*, 197. (c) Hoppen, H.; Muller, E. W.; Kohler, C. P.; Spiering, H.; Meirsner, E.; Gütlich, P. *Chem. Phys. Lett.* **1982**, *91*, 348. (d) Mikami, M.; Konno, M.; Saito, Y. *Chem. Phys. Lett.* **1979**, *63*, 566. (e) Kaji, K.; Sorai, M. *Thermochim. Acta* **1985**, *88*, 185. (f) Greenaway, A. M.; Sinn, E. *J. Am. Chem. Soc.* **1978**, *100*, 8080. (g) Cecconi, F.; Vara, D.; Midollini, S.; Orlandini, A.; Sacconi, L. *Inorg. Chem.* **1981**, *20*, 3423. (h) König, E.; Ritter, G.; Kulshreshtha, S. K.; Waigel, J.; Sacconi, L. *Inorg. Chem.* **1984**, *23*, 1241.

(12) Haddad, M. S.; Lynch, M. W.; Federer, W. D.; Hendrickson, D. N. *Inorg. Chem.* **1981**, *20*, 123–131.

(13) (a) Ganguli, P.; Gütlich, P.; Muller, E. W.; Irler, W. *J. Chem. Soc., Dalton Trans.* **1981**, 441. (b) Gütlich, P. In *Mössbauer Spectroscopy Applied to Inorganic Chemistry*, Long, G. J., Ed.; Plenum Press: New York, 1984.

(14) (a) Haddad, M. S.; Federer, W. D.; Lynch, M. W.; Hendrickson, D. N. *J. Am. Chem. Soc.* **1980**, *102*, 1468–1470. (b) Haddad, M. S.; Federer, W. D.; Lynch, M. W.; Hendrickson, D. N. *Inorg. Chem.* **1981**, *20*, 131–139. (c) Federer, W. D.; Hendrickson, D. N. *Inorg. Chem.* **1984**, *23*, 3870–3877.

(15) (a) Decurtins, S.; Gütlich, P.; Kohler, C. P.; Spiering, H.; Hauser, A. *Chem. Phys. Lett.* **1984**, *105*, 1. (b) Decurtins, S.; Gütlich, P.; Kohler, C. P.; Spiering, H. *J. Chem. Soc., Chem. Commun.* **1985**, 430. (c) Decurtins, S.; Gütlich, P.; Hasselbach, K. M.; Hauser, A.; Spiering, H. *Inorg. Chem.* **1985**, *24*, 2174.

(16) Poganuich, P.; Decurtins, S.; Gütlich, P. *J. Am. Chem. Soc.* **1990**, *112*, 3270–3278.

(17) Kahn, O.; Launay, J. P. *Chemtronics* **1988**, *3*, 140–151.

(18) Sorai, M.; Seki, S. *J. Phys. Chem. Solids* **1974**, *35*, 555.

(19) (a) Kaji, K.; Sorai, M. *Thermochim. Acta* **1985**, *88*, 185. (b) Sorai, M.; Maeda, Y.; Oshio, H. *J. Phys. Chem. Solids* **1990**, *51*, 941.

(20) Federer, W. D.; Hendrickson, D. N. *Inorg. Chem.* **1984**, *23*, 3861.

Table I. Crystallographic Data for $[Fe(3\text{-}OEt\text{-}SalAPA)_2](ClO_4)\cdot S$ ($S = C_6H_5Br$, C_6H_5Cl)

	$S = C_6H_5Br$		$S = C_6H_5Cl$	
chem formula	$FeC_{24}H_{43}N_4O_8ClBr$		$FeC_{34}H_{43}N_4O_8Cl_2$	
a, Å	13.666(4)	13.860(4)	13.604(12)	13.834(4)
b, Å	17.554(5)	17.810(5)	17.475(13)	17.706(5)
c, Å	15.537(4)	15.843(3)	15.379(12)	15.767(3)
β, deg	109.20(2)	110.10(2)	109.24(7)	110.11(2)
V, Å^3	3519.9(17)	3672.8(16)	3452(10)	3626(2)
Z	4	4	4	4
fw	806.9	806.9	762.5	762.5
space group	$P2_1/a$	$P2_1/c$	$P2_1/a$	$P2_1/c$
T, K	163	296	158	296
λ, Å	1.541 84[a]	0.710 73[b]	0.710 73[b]	0.710 73[b]
cryst size; mm	0.13 × 0.15 × 0.37	0.13 × 0.15 × 0.37	0.2 × 0.3 × 0.3	0.30 × 0.30 × 0.44
2θ range, deg	4.0–110.0	4.0–45.0	2.0–42.0	4.0–45.0
octants collcd	$+h,+k,\pm l$	$+h,+k,\pm l$	$\pm h,+k,-l$	$\pm h,+k,+l$
tot. no. of reflcns	4986	5246	4111	5107
no. of obsd reflcns	2857[c]	2530[c]	2048[d]	3099[e]
ρ_{calc}, g cm^{-3}	1.52	1.46	1.47	1.40
μ, cm^{-1}	5.97	1.61	6.46	6.15
R[f]	0.068	0.088	0.049	0.072
R_w[f]	0.097	0.090	0.052	0.075

[a] Cu (Kα). [b] Mo(Kα). [c] $I > 6.0\sigma(I)$. [d] $I > 2.58\sigma(I)$. [e] $F_o > 5.0\sigma(F_o)$. [f] $R = \Sigma||F_o| - |F_c||/\Sigma|F_o|$; $R_w = [\Sigma w(|F_o| - |F_c|)^2/[\Sigma_w|F_o|^2]^{1/2}$.

Physical Measurements. Variable-temperature magnetic susceptibilities were measured on a SQUID susceptometer (SHE Corp. VTS-50). The temperature was controlled using a SHE temperature control device. The magnetic field was set at 10 kG. The cell sample was made of Delrin plastic. A background correction was determined by running a blank cell under experimental conditions and subtracting this background from the sample susceptibilities. Pascal's constants were used as diamagnetic corrections in the calculation of the molar paramagnetic susceptibilities.

^{57}Fe Mössbauer spectra were obtained on a previously described apparatus.[21] The absolute temperature precision is estimated to be ±3 K; the relative precision is ±0.5 K. Mössbauer absorptions were least-squares fit to Lorentzian line shapes with a previously documented computer program.[22] Isomer shift data are reported relative to iron foil at 298 K, but are not corrected for temperature-dependent second-order Doppler effects.

X-band EPR spectra were obtained on a Varian E-9 spectrometer with a gas-flow insert. Sample temperatures were maintained with a Varian V-4540 temperature controller. The temperature accuracy is estimated to be ±5 K. A sample temperature of liquid nitrogen (77 K) was achieved with a direct immersion dewar which was inserted into the cavity.

Powder X-ray diffraction patterns were collected on a Norelco diffractometer with a Cu Kα radiation source on a graphite monochromator. The scan rate was 1 deg/min.

Structure Determinations

$[Fe(3\text{-}OEt\text{-}SalAPA)_2](ClO_4)\cdot C_6H_5Cl$. Black-colored brick-shaped crystals of the C_6H_5Cl solvate suitable for X-ray structure determination were grown by slow evaporation of a CH_2Cl_2 solution containing C_6H_5Cl. The X-ray structure was determined at 158 and 296 K. Crystal, data collection, and refinement parameters are given in Table I.

In the case of the 296 K structure diffraction data were collected on a Nicolet R3 diffractometer at the University of Delaware. A graphite monochromator was used. Systematic absences in the diffraction data uniquely established the space group as $P2_1/c$. The data were corrected for Lorentz and polarization effects; however, no absorption correction was made. The structure was solved by direct methods which located the Fe atom. The remaining non-hydrogen atoms were located by subsequent difference Fourier synthesis. All non-hydrogen atoms were refined anisotropically. All hydrogen atoms were incorporated as idealized, isotropic contributions [d(C–H) = 0.96 Å]. All computer programs and the sources of the scattering factors are contained in the SHELXTL program library 5.1 (G. Sheldrick, Nicolet Corp., Madison, WI). The final difference Fourier map had no significant features. Positional parameters are given in Table II.

Since we knew from a variety of data (*vide infra*) that the C_6H_5Cl solvate makes a relatively abrupt change in spin state at ~178 K, it was decided to determine the structure at a lower temperature, *i.e.*, 158 K. A second crystal was used for data collection at 158 K on an Enraf-Nonius CAD4 diffractometer. This second crystal was first checked to establish that it was $P2_1/c$ at room temperature and that it had the same unit cell as the first crystal. The crystal diffracted well from 2.0 to 42.0° in 2θ. Previous experiments with crystals of this compound indicated that slow cooling through the phase transition might damage the sample, so the temperature was lowered from room temperature to 158 K in approximately 5 min. Despite this precaution, the mosaic spread of the crystal increased upon cooling. No problems were encountered for the data collection, and there was no change in the appearance of the sample during the experiment. The data were corrected for Lorentz and polarization effects. A numerical absorption correction was applied with minimum and maximum transmission factors of 0.870 and 0.894, respectively.

The 158 K structure was solved by direct methods (SHELX-86); correct positions for the non-hydrogen atoms were deduced from an E-map. Subsequent least-squares difference Fourier calculations revealed positions for the hydrogen atoms; however, owing to the paucity of data, hydrogen atoms (except H(11a)–H(12b) and H(25a)–H(26b)) were included as fixed contributors in "idealized" positions. In the final cycle of least squares, carbon atoms were refined with isotropic thermal coefficients, the remaining non-hydrogen atoms were refined with anisotropic thermal coefficients and a group isotropic thermal parameter was varied for the hydrogen atoms. Successful convergence was indicated by the maximum shift/error for the last cycle. The final difference Fourier map had no significant features. A final analysis of variance between observed and calculated structure factors showed no apparent systematic errors. Positional parameters for the 158 K C_6H_5Cl solvate structure are given in Table III.

In cooling the C_6H_5Cl solvate from 296 to 158 K it was found that this crystal dramatically changes from one phase to another phase. The room-temperature $P2_1/c$ setting of the crystal changes fairly abruptly in the region of ~188 K to a $P2_1/a$ setting. As is delineated in the following paper, there is a change in the

(21) Cohn, M. J.; Timken, M. D.; Hendrickson, D. N. *J. Am. Chem. Soc.* **1984**, *106*, 6683.
(22) Chrisman, B. L.; Tumolillo, T. A. *Comput. Phys. Commun.* **1971**, *2*, 322.

Table II. Positional Parameters of $P2_1/c$ Symmetry for $[Fe(3\text{-}OEtSalAPA)_2](ClO_4)\cdot C_6H_5Cl$ at 296 K

	x/a	*y/b*	*z/c*
Fe	0.2400(7)	0.7681(6)	0.2392(7)
O(1)	0.1384(3)	0.7468(2)	0.2928(3)
O(2)	−0.0308(4)	0.6866(3)	0.3017(4)
O(3)	0.3413(3)	0.7896(3)	0.1848(3)
O(4)	0.5116(4)	0.8506(3)	0.1816(4)
N(1)	0.2483(4)	0.8777(3)	0.2915(4)
N(2)	0.3678(4)	0.7498(3)	0.3642(4)
N(3)	0.2330(4)	0.6588(3)	0.1867(4)
N(4)	0.1121(4)	0.7897(4)	0.1128(4)
C(1)	0.0700(5)	0.7937(4)	0.3052(4)
C(2)	0.0870(5)	0.8712(4)	0.3193(5)
C(3)	0.0129(6)	0.9167(5)	0.3360(5)
C(4)	−0.0768(6)	0.8875(5)	0.3384(6)
C(5)	−0.0944(5)	0.8098(5)	0.3265(5)
C(6)	−0.0234(5)	0.7632(4)	0.3114(5)
C(7)	0.1803(6)	0.9056(4)	0.3211(6)
C(8)	0.3467(5)	0.9187(4)	0.3120(6)
C(9)	0.4247(6)	0.8842(5)	0.3981(6)
C(10)	0.4566(5)	0.8032(5)	0.3885(6)
C(11)	0.3955(7)	0.6742(5)	0.4007(6)
C(12)	0.3439(7)	0.7237(6)	0.4438(6)
C(13)	−0.1221(6)	0.6523(5)	0.3059(7)
C(14)	−0.1102(8)	0.5719(6)	0.3059(10)
C(15)	0.4117(5)	0.7433(4)	0.1759(4)
C(16)	0.3972(5)	0.6646(4)	0.1643(5)
C(17)	0.4729(6)	0.6199(5)	0.1494(5)
C(18)	0.5623(6)	0.6504(5)	0.1482(6)
C(19)	0.5786(5)	0.7268(5)	0.1590(5)
C(20)	0.5050(5)	0.7737(4)	0.1724(5)
C(21)	0.3020(5)	0.6300(4)	0.1599(5)
C(22)	0.1329(6)	0.6190(4)	0.1624(6)
C(23)	0.0575(6)	0.6545(5)	0.0768(6)
C(24)	0.0255(5)	0.7335(5)	0.0882(6)
C(25)	0.0812(6)	0.8664(5)	0.0837(6)
C(26)	0.1350(6)	0.8213(5)	0.0361(6)
C(27)	0.6049(6)	0.8858(5)	0.1805(8)
C(28)	0.5947(8)	0.9673(6)	0.1914(11)
Cl(1)	−0.2565(2)	0.5755(1)	−0.0071(2)
O(5)	−0.1798(5)	0.5290(4)	−0.0122(7)
O(6)	−0.3342(4)	0.5344(4)	0.0051(7)
O(7)	−0.2909(8)	0.6206(7)	−0.0818(6)
O(8)	−0.2157(9)	0.6163(8)	0.0706(6)
C(29)	0.2284(7)	0.0471(6)	−0.0358(8)
C(30)	0.2960(8)	0.0316(9)	0.0468(9)
C(31)	0.3340(8)	0.0970(9)	0.0969(10)
C(32)	0.3087(8)	0.1698(8)	0.0668(10)
C(33)	0.2412(8)	0.1803(7)	−0.0174(10)
C(34)	0.1984(7)	0.1165(6)	−0.0728(9)
Cl(2)	0.1766(3)	−0.0320(2)	−0.1049(3)

positions of one half of the C_6H_5Cl solvate molecules. It must be emphasized that the $P2_1/a$ setting for the 158 K structure is **not** just a crystallographically nonstandard formulation of the 296 K $P2_1/c$ unit cell. There is a phase transition. In fact, a crystal of the C_6H_5Cl solvate has been investigated carefully at several temperatures in and around the ~188 K phase transition. The results of this detailed examination are given in the following paper, where the nature of the phase transitions in the whole series of complexes is discussed.

$[Fe(3\text{-}OEt\text{-}SalAPA)_2](ClO_4)\cdot C_6H_5Br$. The X-ray structure of this complex was determined at 163 and 295 K. A dark, prismatic crystal (0.13 × 0.15 × 0.37 mm) was used for data collection at 295 K at the University of California, San Diego, CA, using a Siemens R3m/V diffractometer. A highly oriented graphite crystal monochromator was used. The unit cell dimensions were obtained from 31 reflections which decreased less than 1% during 88 h of X-ray exposure. A face-indexed numerical absorption correction was used with maximum and minimum transmission factors of 0.8726 and 0.8102, respectively. No corrections for the presence of extinctions were made since none were observed. The parameters which characterize the crystal, the data collection, and the refinement are given in Table I.

Table III. Positional Parameters of $P2_1/c$ Symmetry for $[Fe(3\text{-}OEtSalAPA)_2](ClO_4)\cdot C_6H_5Cl$ at 158 K

	x/a	*y/b*	*z/c*
Fe1	0.0	0.0	0.5
O1	−0.1073(4)	0.0272(3)	0.5439(4)
O2	−0.2882(4)	0.0835(3)	0.5370(4)
N1	0.0200(5)	−0.0978(4)	0.5669(4)
N2	0.1117(5)	0.0409(3)	0.6147(5)
C1	−0.1741(6)	−0.0210(5)	0.5625(6)
C2	−0.1503(6)	−0.0981(5)	0.5872(5)
C3	−0.2192(6)	−0.1438(5)	0.6149(5)
C4	−0.3128(6)	−0.1138(5)	0.6173(6)
C5	−0.3377(6)	−0.0375(5)	0.5924(6)
C6	−0.2708(6)	0.0080(5)	0.5642(5)
C7	−0.0487(6)	−0.1295(5)	0.5982(5)
C8	0.1244(6)	−0.1324(5)	0.5987(6)
C9	0.1946(6)	−0.0854(5)	0.6781(6)
C10	0.2105(6)	−0.0040(5)	0.6528(6)
C11	0.0804(7)	0.0769(5)	0.6895(6)
C12	0.1282(8)	0.1245(5)	0.6345(7)
C13	−0.3849(6)	0.1161(5)	0.5364(6)
C14	−0.3959(7)	0.1928(5)	0.4929(6)
Fe2	0.0	0.0	0.0
O3	−0.0929(4)	−0.0221(3)	0.0627(4)
O4	−0.2511(4)	−0.0903(3)	0.0893(4)
N3	−0.0080(5)	0.1097(4)	0.0260(4)
N4	0.1244(4)	−0.0014(4)	0.1193(4)
C15	−0.1701(6)	0.0227(5)	0.0662(5)
C16	−0.1692(6)	0.1025(5)	0.0597(5)
C17	−0.2509(6)	0.1462(5)	0.0702(6)
C18	−0.3361(7)	0.1110(5)	0.0814(6)
C19	−0.3397(6)	0.0316(5)	0.0866(6)
C20	−0.2583(6)	−0.0119(5)	0.0806(6)
C21	−0.0799(6)	0.1413(5)	0.0517(5)
C22	0.0855(6)	0.1579(5)	0.0352(6)
C23	0.1711(6)	0.1369(5)	0.1238(6)
C24	0.2099(6)	0.0556(4)	0.1300(6)
C25	0.1037(7)	−0.0124(5)	0.2077(6)
C26	0.1596(8)	−0.0731(6)	0.1735(7)
C27	−0.3390(7)	−0.1291(5)	0.1024(7)
C28	−0.3086(7)	−0.2127(5)	0.1180(6)
Cl1	0.0210(2)	0.6825(1)	0.7825(2)
O5	0.0882(5)	0.7316(3)	0.7527(4)
O6	−0.0769(4)	0.7196(4)	0.7673(5)
O7	0.0067(6)	0.6130(3)	0.7308(5)
O8	0.0680(4)	0.6668(4)	0.8783(4)
Cl2	0.1211(2)	0.7814(2)	0.3641(2)
C29	0.0562(6)	0.7001(5)	0.3079(6)
C30	0.0841(7)	0.6293(5)	0.3493(6)
C31	0.0360(7)	0.5655(6)	0.3031(6)
C32	−0.0386(7)	0.5720(5)	0.2184(7)
C33	−0.0673(7)	0.6422(6)	0.1776(7)
C34	−0.0196(7)	0.7087(6)	0.2235(7)

The 295 K structure was solved using direct methods (Siemens SHELXTL PLUS) on a Micro VAXII computer. Phenyl rings were constrained to ideal regular hexagons. Hydrogen atoms were included in ideal positions with an isotropic thermal parameter fixed at 0.08. A residual peak (1.39 e $Å^{-3}$, at 0.839, 0.539, 0.575) was located near the bromine atom. No evidence of secondary extinction was observed. The relatively large observed R values are due to large thermal motion of both the ClO_4^- anion and bromobenzene molecule and indicates possible disordering of both. Positional parameters for the 295 K structure are given in Table IV.

The same crystal was used for the 163 K structure. Unit cell parameters (Table I) were obtained using 15 reflections. A face-indexed numerical absorption correction was carried out with maximum and minimum transmission factors of 0.577 and 0.383, respectively. The 163 K structure was also solved using direct methods (Siemens SHELXTL Plus) on a Micro VAX II computer. Hydrogen atom positions were defined using a riding model with fixed isotropic thermal parameters in idealized positions. The final difference Fourier map for the 163 K structure had no significant features. Table V gives the positional parameters for the 163 K structure.

Table IV. Positional Parameters of $P2_1/c$ Symmetry for $[Fe(3\text{-}OEt\text{-}SalAPA)_2](ClO)_4 \cdot C_6H_5Br$ at 295 K

	x/a	y/b	z/c
Br	0.6708(2)	0.5305(2)	0.3917(2)
Fe	0.2603(1)	0.2324(1)	0.7601(1)
Cl	0.2422(3)	-0.0728(3)	0.4922(3)
O(1)	0.3618(6)	0.2544(5)	0.7067(6)
O(2)	0.5318(7)	0.3143(6)	0.6974(7)
O(3)	0.1595(6)	0.2099(5)	0.8145(5)
O(4)	0.0099(7)	0.1475(6)	0.8180(6)
O(5)	0.2060(11)	-0.1163(9)	0.4198(10)
O(6)	0.1655(8)	-0.0327(7)	0.5054(10)
O(7)	0.3190(9)	-0.0263(7)	0.4870(10)
O(8)	0.2832(13)	-0.1154(9)	0.5675(10)
N(1)	0.2524(8)	0.1235(6)	0.7064(6)
N(2)	0.1342(8)	0.2494(6)	0.6358(7)
N(3)	0.2676(8)	0.3399(6)	0.8128(7)
N(4)	0.3894(8)	0.2126(7)	0.8857(7)
C(1)	0.4318(6)	0.2067(5)	0.6926(6)
C(2)	0.4139(6)	0.1298(5)	0.6800(6)
C(3)	0.4869(6)	0.0837(5)	0.6635(6)
C(4)	0.5778(6)	0.1147(5)	0.6596(6)
C(5)	0.5956(6)	0.1916(5)	0.6722(6)
C(6)	0.5226(6)	0.2377(5)	0.6887(6)
C(7)	0.3203(10)	0.0965(8)	0.6779(9)
C(8)	0.1551(11)	0.0821(8)	0.6869(11)
C(9)	0.0752(11)	0.1163(9)	0.6045(11)
C(10)	0.0444(11)	0.1965(8)	0.6119(10)
C(11)	0.1570(12)	0.2732(10)	0.5576(9)
C(12)	0.1045(13)	0.3241(10)	0.5988(11)
C(13)	0.6238(12)	0.3486(10)	0.6947(14)
C(14)	0.6134(16)	0.4259(12)	0.6966(18)
C(15)	0.0876(6)	0.2567(5)	0.8246(6)
C(16)	0.1033(6)	0.3339(5)	0.8357(6)
C(17)	0.0286(6)	0.3793(5)	0.8504(6)
C(18)	-0.0618(6)	0.3475(5)	0.8541(6)
C(19)	-0.0775(6)	0.2701(5)	0.8430(6)
C(20)	-0.0028(6)	0.2247(5)	0.8282(6)
C(21)	0.1986(11)	0.3687(8)	0.8371(9)
C(22)	0.3655(12)	0.3803(9)	0.8355(11)
C(23)	0.4435(11)	0.3425(10)	0.9208(11)
C(24)	0.4760(10)	0.2666(9)	0.9116(9)
C(25)	0.4196(12)	0.1331(10)	0.9157(10)
C(26)	0.3661(13)	0.1811(10)	0.9626(10)
C(27)	-0.1032(14)	0.1155(10)	0.8180(13)
C(28)	-0.0923(16)	0.0347(12)	0.8081(19)
C(29)	0.7300(11)	0.4513(9)	0.4642(12)
C(30)	0.7985(11)	0.4589(9)	0.5520(12)
C(31)	0.8383(11)	0.3952(9)	0.6034(12)
C(32)	0.8096(11)	0.3239(9)	0.5669(12)
C(33)	0.7412(11)	0.3163(9)	0.4792(12)
C(34)	0.7014(11)	0.3800(9)	0.4278(12)

As with the C_6H_5Cl solvate, the C_6H_5Br solvate crystal also changes from a $P2_1/c$ phase at room temperature to a $P2_1/a$ phase at 163 K. The same type of shift in one half of the solvate molecules occurs. In the following paper where the phase transitions are investigated it will be shown that the transformation from one phase to the other occurs relatively abruptly at the temperature where a sharp heat capacity effect is observed.

$[Fe(3\text{-}OEt\text{-}SalAPA)_2](ClO_4)\cdot o\text{-}C_6H_4Cl_2$. The X-ray structure of this complex was only determined at 295 K. A dark, clear, rectangular crystal was used for data collection on a Siemens R3m/V diffractometer at the University of California, San Diego, CA. The unit cell dimensions were obtained from 17 reflections. The intensities of the monitored reflections decreased less than 1% during 37 h of X-ray exposure. No corrections for the presence of extinctions were made, since none were observed. A face-indexed numerical absorption correction was used with maximum and minimum transmission factors of 0.630 and 0.380, respectively. The parameters which characterize the crystal, the data collection, and the refinement are given in Table VI. For comparison purposes the same parameters are also given for the benzene solvate $[Fe(3\text{-}OEt\text{-}SalAPA)_2](ClO_4)\cdot C_6H_6$ at 128 and 298 K. Previously we reported[23] the structure of this complex at five different temperatures from 20 to 300 K. The C_6H_6 and $o\text{-}C_6H_4Cl_2$ solvates both crystallize in the $C2/c$ space group at room temperature.

Table V. Positional Parameters of $P2_1/a$ Symmetry for $[Fe(3\text{-}OEtSalAPA)_2](ClO_4)\cdot C_6H_5Br$ at 163 K

	x/a	y/b	z/c
Br	0.1233(1)	0.2159(1)	0.3617(1)
Fe(1)	0.0	0.0	0.5000
Fe(2)	0.5000	0.5000	0.0
Cl	0.0205(2)	0.3162(1)	-0.2176(2)
O(1)	0.1077(5)	0.0269(3)	0.4535(5)
O(2)	0.2883(5)	0.0830(3)	0.4620(4)
O(3)	0.4068(5)	0.4773(3)	0.0626(4)
O(4)	0.2471(5)	0.4095(3)	0.0870(4)
O(5)	0.0052(8)	0.3837(5)	-0.2691(6)
O(6)	0.0887(6)	0.2677(5)	-0.2460(5)
O(7)	-0.0749(6)	0.2790(5)	-0.2310(6)
O(8)	0.0675(6)	0.3331(5)	-0.1220(5)
N(1)	-0.0178(6)	-0.0997(4)	0.4308(5)
N(2)	-0.1164(6)	0.0389(4)	0.3812(5)
N(3)	0.4926(6)	0.6094(4)	0.0263(5)
N(4)	0.3759(6)	0.5011(4)	-0.1193(6)
C(1)	0.1747(8)	-0.0203(5)	0.4353(7)
C(2)	0.1503(7)	-0.0976(5)	0.4098(7)
C(3)	0.2218(8)	-0.1427(6)	0.3832(7)
C(4)	0.3136(8)	-0.1135(6)	0.3831(7)
C(5)	0.3395(7)	-0.0365(6)	0.4093(8)
C(6)	0.2726(7)	0.0080(6)	0.4378(6)
C(7)	0.0507(7)	-0.1287(5)	0.4003(7)
C(8)	-0.1216(7)	-0.1360(6)	0.3998(7)
C(9)	-0.1924(7)	-0.0890(5)	0.3207(7)
C(10)	-0.2127(8)	-0.0087(5)	0.3468(8)
C(11)	-0.1357(8)	0.1218(5)	0.3627(7)
C(12)	-0.0862(9)	0.0751(5)	0.3079(7)
C(13)	0.3863(8)	0.1151(6)	0.4636(7)
C(14)	0.3972(9)	0.1937(6)	0.5093(8)
C(15)	0.3287(7)	0.5226(5)	0.0661(6)
C(16)	0.3327(7)	0.6023(5)	0.0615(7)
C(17)	0.2494(8)	0.6465(6)	0.0713(7)
C(18)	0.1650(8)	0.6119(6)	0.0810(7)
C(19)	0.1605(8)	0.5312(6)	0.0858(7)
C(20)	0.2408(8)	0.4894(5)	0.0789(7)
C(21)	0.4215(7)	0.6404(5)	0.0540(6)
C(22)	0.4127(7)	0.3414(5)	-0.0374(6)
C(23)	0.3296(8)	0.3631(6)	-0.1256(7)
C(24)	0.2920(7)	0.4458(5)	-0.1304(7)
C(25)	0.3424(9)	0.5724(6)	-0.1707(7)
C(26)	0.3976(9)	0.5150(6)	-0.2047(7)
C(27)	0.1624(8)	0.3717(6)	0.1031(8)
C(28)	0.1901(9)	0.2891(6)	0.1146(8)
C(29)	0.0524(8)	0.3046(6)	0.3021(8)
C(30)	0.0801(8)	0.3737(6)	0.3451(8)
C(31)	0.0325(9)	0.4394(7)	0.2991(8)
C(32)	-0.0394(10)	0.4342(7)	0.2163(9)
C(33)	-0.0688(10)	0.3635(7)	0.1717(9)
C(34)	-0.0205(9)	0.2975(7)	0.2183(8)

The 295 K structure of $[Fe(3\text{-}OEt\text{-}SalAPA)_2](ClO_4)\cdot o\text{-}C_6H_4Cl_2$ was solved using Patterson map techniques (Siemens SHELXTL PLUS) on a Micro VAX II computer. Data were refined employing a full-matrix least-squares method. Hydrogen atom positions were fixed in idealized positions with isotropic thermal parameters of 0.08 Å^3. Positional parameters are given in Table VII.

Observed and calculated structure factors as well as tables of anisotropic thermal parameters and calculated hydrogen positions for the above five X-ray structure determinations are available in the supplementary materials.

Results and Discussion

Spin-Crossover Solvate Series. The main goal of this work was to add to our understanding of how a solvate molecule in the

(23) Timken, M. D.; Strouse, C. E.; Soltis, S. M.; Daverio, S. A.; Hendrickson, D. N.; Abdel-Mawgoud, A. M.; Wilson, S. R. *J. Am. Chem. Soc.* **1986**, *108*, 395–402.

Table VI. Crystallographic Data for $[Fe(3\text{-}OEt\text{-}SalAPA)_2]\text{-}(ClO_4)_2\cdot S$ (S = C_6H_6 or $C_6H_4Cl_2$)

	S = C_6H_6		S = $C_6H_4Cl_2$
chem formula	$FeC_{34}H_{44}N_4O_8Cl$		$FeC_{34}H_{42}N_4O_8Cl_3$
a, Å	16.54(1)	16.960(4)	17.187(8)
b, Å	17.35(1)	17.600	17.807(7)
c, Å	13.46(1)	13.832	13.899(8)
β, deg	119.267(18)	119.030(5)	119.94(4)
V, Å^3	3370	3610	3686(3)
Z	4	4	4
fw	727.4	727.4	796.2
space group	$P2_1/c$	$C2/c$	$C2/c$
T, K	128	298	298
λ, Å	0.710 73[a]	0.710 73[a]	1.541 84[b]
cryst size, mm	0.18 × 0.18 × 0.31	0.18 × 0.18 × 0.31	0.08 × 0.15 × 0.37
2θ range, deg	−50.0	−50.0	2.0–110.0
octants collcd			$+h,+k,\pm l$
tot. no. of reflcns	6306	6723	2493
no. of obsd reflcns	3654[c]	1318[c]	1801[d]
ρ_{calc}, g cm^{-3}	1.43	1.34	1.44
μ, cm^{-1}		5.63	5.80
R[e]	0.062	0.071	0.055
R_w[f]	0.072	0.082	0.076

[a] Mo (Kα). [b] Cu (Kα). [c] $I > 3\sigma(I)$. [d] $I > 5\sigma(I)$. [e] $R = \sum||F_o| - |F_c||/\sum|F_o|$. [f] $R_w = [\sum w(|F_o| - |F_c|)^2/[\sum w|F_o|^2]^{1/2}$.

Table VII. Positional Parameters of $C2/c$ Symmetry for $[Fe(3\text{-}OEtSalAPA)_2](ClO_4)\cdot o\text{-}C_6H_4Cl_2$ at 295 K

	x/a	y/b	z/c
Fe	0.2500	0.2500	0
Cl(1)	0.5000	0.9269(1)	0.2500
Cl(2)	0.5975(2)	0.4717(1)	0.2690(2)
O(1)	0.3038(2)	0.2718(2)	0.1559(2)
O(2)	0.3089(3)	0.3306(2)	0.3322(3)
O(3)	0.5746(5)	0.8838(4)	0.2899(6)
O(4)	0.4920(4)	0.9713(3)	0.1637(4)
N(1)	0.1248(3)	0.2281(3)	0.0016(3)
N(2)	0.3040(3)	0.1426(2)	0.0456(3)
C(1)	0.0477(4)	0.1969(4)	−0.0989(5)
C(2)	0.0946(4)	0.1515(4)	0.0017(5)
C(3)	0.0997(4)	0.2822(3)	0.0634(4)
C(4)	0.0887(4)	0.3618(4)	0.0210(5)
C(5)	0.1711(4)	0.3978(3)	0.0306(5)
C(6)	0.3328(3)	0.1128(3)	0.1429(4)
C(7)	0.3275(3)	0.1469(3)	0.2324(4)
C(8)	0.3435(4)	0.1020(3)	0.3239(4)
C(9)	0.3455(4)	0.1312(4)	0.4143(5)
C(10)	0.3330(4)	0.2069(3)	0.4203(4)
C(11)	0.3185(3)	0.2550(3)	0.3336(4)
C(12)	0.3152(3)	0.2247(3)	0.2369(4)
C(13)	0.3099(5)	0.3636(4)	0.4266(5)
C(14)	0.3035(8)	0.4449(4)	0.4119(7)
C(15)	0.5461(5)	0.5559(4)	0.2594(5)
C(16)	0.5899(6)	0.6231(4)	0.2694(5)
C(17)	0.5448(5)	0.6884(4)	0.2598(6)

crystal of a spin-crossover complex affects the transformation from low- to high-spin states. The series $[Fe(3\text{-}OEt\text{-}SalAPA)_2]\text{-}(ClO_4)\cdot S$ includes the nonsolvated complex (no S) as well as the solvates where S = C_6H_6, C_6H_5Cl, C_6H_5Br, $o\text{-}C_6H_4Cl_2$ or C_6H_5I. The fact that all of these complexes have basically the same packing arrangements in the solid state was initially deduced from powder X-ray diffraction data. Single-crystal X-ray structural results are given in this paper for all of the complexes except the C_6H_5I solvate. At the outset it has to be admitted that we did **not** anticipate just how complicated the structural problem would become. *As it turns out there are at least five different phases observed for the above complexes.*

Powder XRD patterns were determined for five of the six complexes in the series at room temperature (figure available in supplementary material). Examination of these five powder patterns suggested that the five complexes are probably arranged approximately the same way in the solid. The C_6H_5Cl and C_6H_5Br solvates appear to be isostructural. It should be noted that the C_6H_5F solvate was prepared, and from its powder XRD pattern it was found to be structurally quite different than the other complexes. Also, a powder XRD pattern was determined for $[Fe(3\text{-}OEt\text{-}SalAPA)_2]ClO_4$. This nonsolvated complex was found to be isostructural to $[Fe(3\text{-}OMe\text{-}SalAPA)_2]ClO_4$, for which the X-ray structure at 295 K was reported.[24]

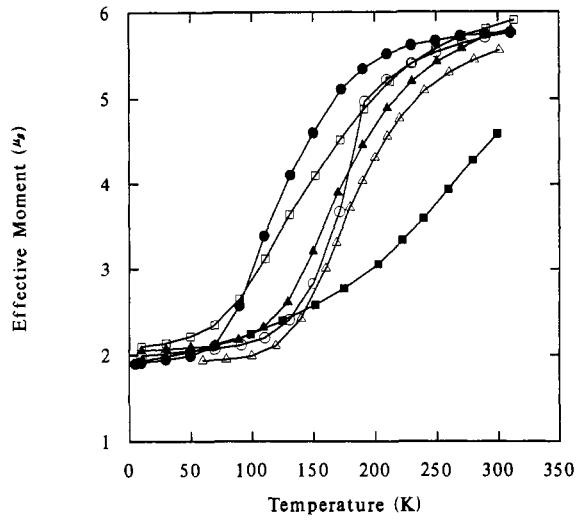

Figure 1. Plots of the effective magnetic moment per iron, μ_{eff}, versus temperature for the complex $[Fe(3\text{-}OEt\text{-}SalAPA)_2](ClO_4)\cdot S$, where the solvate molecule S is either absent (■) or is C_6H_6 (△), C_6H_5Cl (○), C_6H_5Br (□), C_6H_5I (▲), or $o\text{-}C_6H_4Cl_2$ (●).

The best way to demonstrate that all six complexes exhibit a spin-crossover transformation is with magnetic susceptibility data. Figure 1 gives a plot of the effective magnetic moment (μ_{eff}) per iron as a function of temperature. Tables of the magnetic susceptibility data for the five solvates and the nonsolvated complex are available in the supplementary material. Below ~50 K all six complexes are low-spin Fe^{III} complexes with $\mu_{eff} = 2.0$ μ_B. As the temperature is increased all six complexes exhibit a spin-crossover transformation. The nonsolvated complex exhibits the most gradual transformation. The μ_{eff} value for this complex increases gradually from 2.24 μ_B at 98.9 K to 4.60 μ_B at 299.5 K. As deduced from the EPR results (*vide infra*), the low-spin state is one of the Kramers doublets from the $^2T_{2g}$ state. The high-spin state is comprised of three Kramers doublets which are essentially at the same energy. It can also be seen that the degree of abruptness varies from one solvate to another. The C_6H_5I solvate is the least abrupt, and the C_6H_5Cl solvate is the most abrupt. There are at least two basic ways in which the solvate molecule may affect the spin-crossover transformation. In the temperature region where the Fe^{III} complexes convert from low- to high-spin the solvate molecules may convert cooperatively from being static to dynamic in the lattice, where the motion occurs in a phonon mode. The motion of the solvate molecules would make the lattice about each Fe^{III} complex softer, and this could facilitate the relatively large amplitude motion of the Fe^{III} complex as it interconverts between the smaller low-spin form to the larger high-spin form. On the other hand the solvate molecules may serve only as spacers between Fe^{III} complexes. A large spacer may reduce cation–cation interactions and, therefore, affect the cooperativity in the spin-crossover transformation.

Electron Paramagnetic Resonance Spectroscopy. As discussed in previous papers,[20,25] two types of information are available from EPR spectra of spin-crossover complexes. The rate at which each complex interconverts between the low- and high-spin states

(24) Xie, C.-L.; Hendrickson, D. N. Submitted for publication.
(25) Timken, M. D.; Hendrickson, D. N.; Sinn, E. *Inorg. Chem.* **1985**, *24*, 3947–3955.

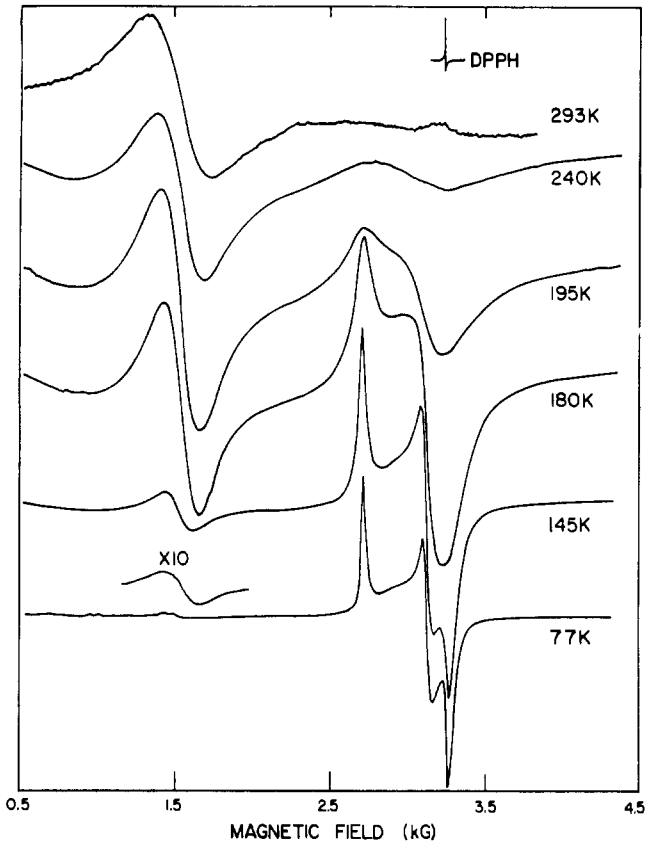

Figure 2. Variable-temperature X-band EPR spectrum of a polycrystalline sample of $[Fe(3\text{-}OEt\text{-}SalAPA)_2](ClO_4)\cdot C_6H_5Cl$.

Table VIII. X-Band EPR Parameters for $Fe(3\text{-}OEtSalAPA)_2](ClO_4)\cdot S$ at 77 K and 295 K[a]

	g-values			
	77 K			
solvate molecule (S)	g_x	g_y	g_z	295 K *g*
C_6H_5Cl	2.363	2.060	1.972	4.12
C_6H_5Br	2.389	2.079	1.977	4.11
C_6H_5I	2.390	2.073	1.978	4.13
$o\text{-}C_6H_4Cl_2$	2.391	2.088	1.973	4.08

[a] Polycrystalline samples were used.

can be gauged relative to the EPR time scale. The nature of the Kramers doublet which serves as the ground state can also be determined.

Variable-temperature X-band EPR spectra were recorded for all of the solvate complexes. Except for shifts in temperatures reflecting the different T_c values for each solvate, the variable-temperature spectra look similar. In Figure 2 are shown representative EPR spectra for the C_6H_5Cl solvate. At 293 K the dominant signal in the spectrum is a broad derivative at g = 4.12. This signal is assignable to Fe^{III} complexes in the high-spin $^6A_1$ state. As the temperature is decreased the g = 4.12 signal losses intensity and a rhombic low-spin Fe^{III} signal increases in intensity. At 77 K this low-spin signal is characterized by g values of 2.363, 2.060, and 1.972. In Table VIII are given the g values obtained at 77 K and room temperature for the five solvate complexes. For all of these complexes decreasing the temperature leads to the low-spin signal gaining in intensity at the expense of the high-spin signal. For each solvate the relative intensity of the two signals as a function of temperature is in qualitative agreement with the changes in high-spin (low-spin) distribution calculated from the magnetic susceptibility data.

One simple conclusion can be made from the EPR spectra illustrated in Figure 2. In the temperature region of ~77 to ~240 K both high- and low-spin EPR signals can be seen. The rate of spin-state interconversion for each Fe^{III} complex is slower at all temperatures than the EPR time scale, *i.e.*, slower than $\sim 10^{10}$ s^{-1}. This same type of observation has been made for several N_4O_2 type Fe^{III} spin-crossover complexes,[14,20,25] and even for S_6 type Fe^{III} spin-crossover complexes (*i.e.*, dithiocarbamates).[26] Laser temperature-jump[27] and ultrasonic relaxation studies[28] have shown that the $Fe^{III}S_6$ spin-crossover complexes exhibit the fastest spin-state interconversion rates.

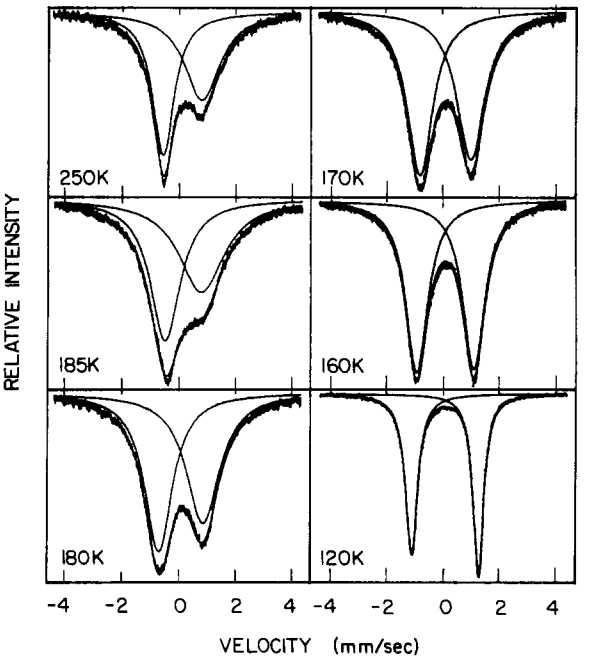

Figure 3. Variable-temperature ^{57}Fe Mössbauer spectrum of a polycrystalline sample of $[Fe(3\text{-}OEt\text{-}SalAPA)_2](ClO_4)\cdot C_6H_5Cl$ prepared by the small-scale preparation scheme (*i.e.*, method I).

The g values for the low-spin state of the $[Fe(3\text{-}OEt\text{-}SalAPA)_2](ClO_4)\cdot S$ series are all similar. They are also similar to those reported[14c,20] for various forms of the analogous unsubstituted complex $[Fe(SalAPA)_2]ClO_4$. For example, the CH_2Cl_2 solvate of the unsubstituted complex has at 77 K g values of 2.355, 2.092 and 1.966.

Mössbauer Spectroscopy. Variable-temperature ^{57}Fe Mössbauer data were taken for all of the solvates prepared either by the small-sample preparation scheme (method I) or by the large sample preparation scheme (method II) used to prepare the quite large samples for heat capacity measurements. In Figure 3 can be found spectra for a sample prepared by method I for the chlorobenzene solvate $[Fe(3\text{-}OEt\text{-}SalAPA)_2](ClO_4)\cdot C_6H_5Cl$, which is representative of the series. Spectra for the other solvates prepared by method I are available in the supplementary material. The fitting parameters for the benzene, chlorobenzene, bromobenzene, and *o*-dichlorobenzene solvates can be found in Tables IX and X. There appears to be only one average quadrupole-split doublet throughout the temperature range. Each spectrum was least-squares fit to two Lorentzian lines with the two components fixed to have equal areas. It is clear that the rate of spin-state interconversion is fast on the Mössbauer timescale, that is, faster than $\sim 10^8$–10^9 s^{-1}.

(26) Hall, G. R.; Hendrickson, D. N. *Inorg. Chem.* **1976**, *15*, 607.
(27) (a) Dwey, T. G.; Turner, D. H. *Adv. Mol. Relax. Interact. Process* **1978**, *13*, 331. (b) Beattie, J. K.; Sutin, N.; Turnder, D. H.; Flynn, G. W. *J. Am. Chem. Soc.* **1973**, *95*, 2052. (c) Hoselton, M. A.; Drago, R. S.; Wilson, L. J.; Sutin, N. *J. Am. Chem. Soc.* **1976**, *98*, 6979. (d) Reeder, K. A.; Dose, E. V.; Wilson, L. J. *Inorg. Chem.* **1978**, *17*, 1071.
(28) (a) Beattie, J. K.; Binstead, R. A.; West, R. J. *J. Am. Chem. Soc.* **1978**, *100*, 3044. (b) Binstead, R. A.; Beattie, J. K.; Dose, E. V.; Tweedle, M. F.; Wilson, L. J. *J. Am. Chem. Soc.* **1978**, *100*, 5609. (c) Binstead, R. A.; Beattie, J. K.; Dewey, T. G.; Turner, D. H. *J. Am. Chem. Soc.* **1980**, *100*, 5609. (d) Beattie, J. K.; McMahon, K. J. *Aust. J. Chem.* **1988**, *41*(9), 1315.

Table IX. Mössbauer Parameters for $[Fe(3\text{-}OEt\text{-}SalAPA)_2](ClO_4)_2 \cdot S$ Where the Solvate Molecule S Is either C_6H_5Cl or C_6H_5Br[a]

T, K	δ, mm s^{-1}	ΔE_Q, mm s^{-1}	$\Gamma_{1/2}(-)$,[b] mm s^{-1}	$\Gamma_{1/2}(+)$,[c] mm s^{-1}	ln (area)[d]
		C_6H_5Cl Solvate			
310	0.313(3)	1.424(3)	0.382(4)	0.632(3)	−0.351
250	0.319(2)	1.383(5)	0.470(3)	0.761(5)	0.972
210	0.298(4)	1.274(5)	0.540(7)	0.886(4)	1.33
190	0.294(3)	1.264(5)	0.617(5)	0.953(4)	1.54
185	0.293(3)	1.277(6)	0.644(4)	0.982(7)	1.60
180	0.227(2)	1.567(4)	0.589(4)	0.716(5)	1.66
170	0.212(5)	1.807(3)	0.550(5)	0.606(6)	1.77
160	0.193(3)	2.023(2)	0.467(4)	0.476(5)	1.84
120	0.165(3)	2.372(3)	0.255(8)	0.225(9)	2.01
		C_6H_5Br Solvate			
340	0.323(2)	1.537(5)	0.348(5)	0.505(4)	0.151
300	0.326(3)	1.513(5)	0.417(5)	0.620(6)	0.739
260	0.322(4)	1.394(5)	0.476(4)	0.731(6)	1.21
220	0.294(2)	1.305(4)	0.538(3)	0.822(6)	1.62
200	0.267(3)	1.379(3)	0.561(4)	0.792(3)	1.77
190	0.250(5)	1.495(4)	0.575(5)	0.759(5)	1.88
170	0.217(2)	1.841(4)	0.593(4)	0.671(5)	2.07
140	0.174(2)	2.326(2)	0.402(5)	0.394(6)	2.23
110	0.165(3)	2.466(2)	0.274(6)	0.259(6)	2.31

[a] Both samples were prepared by the small scale method I. Parameters were obtained by assuming equal areas for the two components peaks of a given quadrupole doublet. [b] Half-width at half-height of the negative-velocity quadrupolar component. [c] Half-width at half-height of the positive-velocity quadrupolar component. [d] Natural logarithm of background-normalized area of total fitted spectrum.

Table X. Mössbauer Parameters for $[Fe(3\text{-}OEt\text{-}SalAPA)_2](ClO_4) \cdot S$ Where the Solvate Molecule S Is either $o\text{-}C_6H_4Cl_2$ or C_6H_6[a]

T, K	δ, mm s^{-1}	ΔE_Q, mm s^{-1}	$\Gamma_{1/2}(-)$,[b] mm s^{-1}	$\Gamma_{1/2}(+)$,[c] mm s^{-1}	ln (area)[d]
		$o\text{-}C_6H_4Cl_2$ Solvate			
310	0.324(2)	1.634(4)	0.405(3)	0.657(4)	0.477
230	0.337(2)	1.571(4)	0.490(2)	0.811(3)	1.12
200	0.333(2)	1.467(5)	0.622(3)	1.04(3)	1.49
180	0.321(3)	1.371(2)	0.771(3)	1.27(3)	1.68
170	0.315(1)	1.367(4)	0.854(3)	1.34(5)	1.76
155	0.246(1)	1.531(3)	0.932(5)	1.20(4)	1.84
145	0.218(2)	1.816(3)	0.886(3)	1.01(4)	1.85
130	0.187(3)	2.208(3)	0.703(4)	0.703(6)	1.87
110	0.176(2)	2.447(2)	0.454(3)	0.405(6)	1.93
		C_6H_6 Solvate			
306	0.317(1)	1.481(3)	0.332(2)	0.508(3)	1.090
274	0.337(2)	1.381(3)	0.402(2)	0.616(4)	1.510
245	0.365(2)	1.267(5)	0.466(3)	0.728(6)	1.841
224	0.348(2)	1.199(4)	0.483(3)	0.737(6)	1.995
205	0.334(2)	1.284(4)	0.520(3)	0.699(5)	1.797
195	0.322(1)	1.414(3)	0.534(2)	0.663(3)	1.881
185	0.314(1)	1.600(3)	0.545(3)	0.616(3)	1.970
173	0.309(1)	1.792(2)	0.556(2)	0.600(3)	2.067
159	0.291(1)	2.084(2)	0.462(2)	0.453(2)	2.152
145	0.284(1)	2.274(2)	0.371(2)	0.342(2)	2.199
129	0.282(1)	2.360(3)	0.307(3)	0.279(2)	2.209
111	0.287(1)	2.389(3)	0.277(3)	0.254(3)	2.219

[a] Both samples were prepared by the small scale method I. Parameters were obtained by assuming equal areas for the two components of a given quadrupole doublet. [b] Half-width at half-height of the negative-velocity component. [c] Half-width at half-height of the positive-velocity component. [d] Natural logarithm of background-normalized area of total fitted spectrum.

^{57}Fe Mössbauer spectra were also run for portions of the large samples employed in the heat capacity measurements. Since these large scale (17–20 g) preparations were carried out in a somewhat different manner than the small scale preparations, it was important to see if the physical properties were different. Variable-temperature Mössbauer spectra which are characteristic of the large-scale samples are shown in Figures 4 and 5 for the C_6H_5Br and $o\text{-}C_6H_4Cl_2$ solvates, respectively. It is clear from Figure 4 that in the range 110–180 K two distinct quadrupole-split doublets can be seen for the C_6H_5Br solvate. This suggests that in this temperature region the high- and low-spin species are interconverting at a rate slower than $\sim 10^6$ s^{-1}. There is also observed a gradual broadening of the signals from 180 to 250 K. The spectra were least-squares fit to two sets of Lorentzian line shapes (*i.e.*, two doublets). A similar temperature dependence is seen in Figure 5 for the *o*-dichlorobenzene solvate. The fact

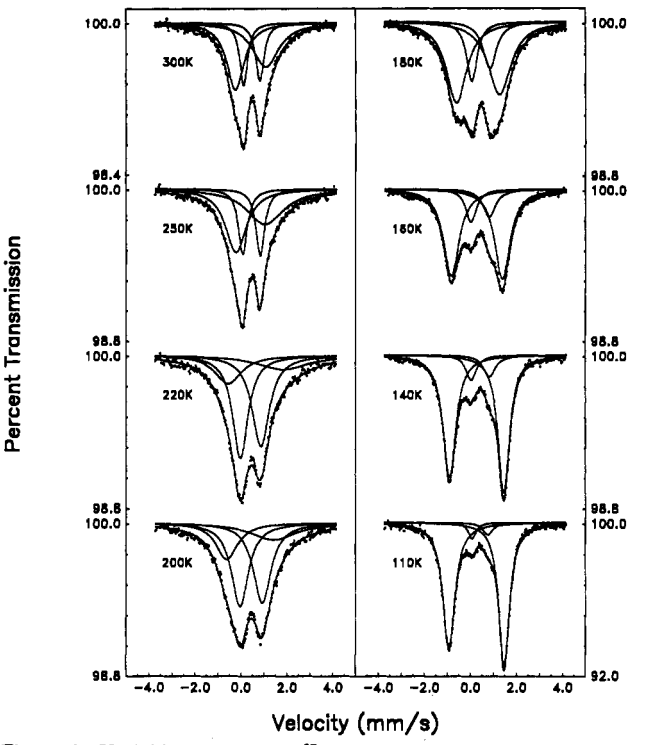

Figure 4. Variable-temperature ^{57}Fe Mössbauer spectrum of a polycrystalline sample of $[Fe(3\text{-}OEt\text{-}SalAPA)_2](ClO_4) \cdot C_6H_5Br$ prepared by the large-scale method II. This sample was a portion of the material used for the heat capacity measurements, see following paper.

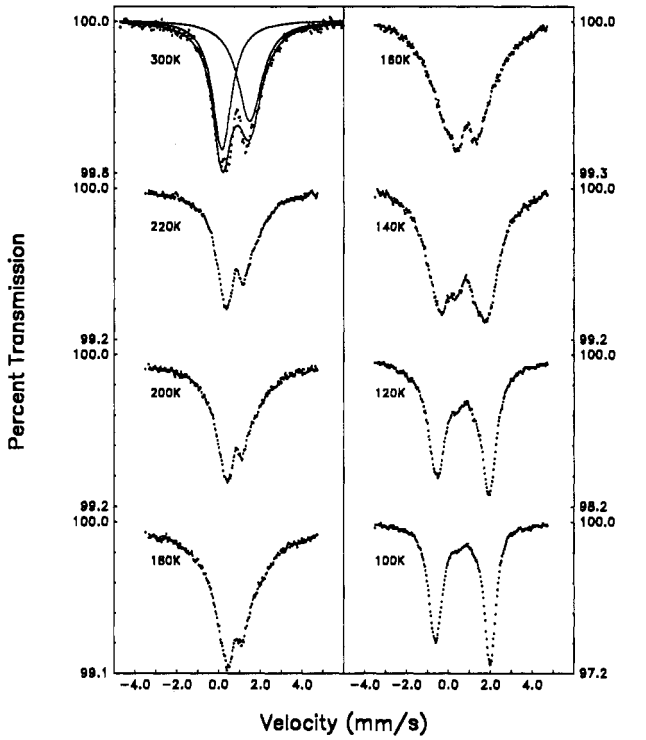

Figure 5. Variable-temperature ^{57}Fe Mössbauer spectrum of a polycrystalline sample of $[Fe(3\text{-}OEt\text{-}SalAPA)_2](ClO_4) \cdot o\text{-}C_6H_4Cl_2$ prepared by the large-scale method II. This sample was a portion of the material used for the heat capacity measurements, see following paper.

that the broadening and changes occurring in the Mössbauer line shapes for the bromobenzene solvate occur at higher temperatures than those observed for the *o*-dichlorobenzene solvate suggests that the broadening is associated with the spin-crossover process.

Broadening of Mössbauer line shapes can be attributed to either inhomogeneous broadening effects or relaxation phenomena. In the first case, broadening occurs as a result of a distribution of environments in which the iron complexes reside. It can be seen that the line broadenings observed for each of the solvates prepared in large scale, C_6H_5Cl, C_6H_5Br, C_6H_6, and $C_6H_4Cl_2$, is greatest in the temperature region where the spin-state interconversion is most abrupt as established by the magnetic susceptibility results.

Line-shape broadening effects have been observed before in spin-crossover systems.[11h,29] In one case[11h] an order-disorder process involving the acetone solvate molecules of a ferrous spin-crossover complex, $[Fe(dppen)_2Cl_2](ClO_4)\cdot 2(CH_3)CO$, was thought to induce broadening of the Mössbauer absorption lines. The authors observed an increase in both the low- and high-spin Mössbauer linewidths below a critical transition temperature. Below the transition temperature the solvate molecules are sitting in two different lattice sites, as evidenced by X-ray crystallography, whereas above this temperature the solvate molecules occupy only one type of lattice site. Thus, one could observe a Mössbauer signal as a superposition of two doublets arising from the two types of Fe^{II} complexes below the transition temperature. If the two lattice sites are not very different, then the two doublets would have similar parameters and could be close to each other. The effect could appear as line broadening. At the transition temperature, it was suggested that the acetone solvate molecules convert from being static to dynamic in an order-disorder phase transition. The Mössbauer line shapes would be expected to sharpen as the sample temperature is increased if the disordering was fast on the Mössbauer time scale.

Coalescence and broadening of the line shapes may also occur when the high- and low-spin complexes interconvert at a rate which is comparable to the Mössbauer time scale. This type of behavior has been seen for several ferric spin-crossover complexes by Maeda *et al.*[29] A simulation of the Mössbauer spectra was carried out, in which a quantum mechanical density matrix formalism developed by Wickman[30] was applied, in order to determine the spin-crossover rates directly.

Many examples of N_4O_2 ferric spin-crossover complexes which undergo fast spin-interconversion on the Mössbauer time scale have been reported.[14c,20,23,24] Federer and Hendrickson[14c,20] studied the nonsolvated form of $[Fe(SalAPA)_2]ClO_4$ and observed, among other things, the effects of sample preparation and grinding on the spin-crossover rates. Sample grinding effects have also been reported[3i,31] for other spin-crossover complexes. For example, when $[Fe(SaAPA)_2]ClO_4$ is well crystallized, only a single average doublet is seen at all temperatures. The complex is interconverting faster than the Mössbauer time scale. However, it was also reported[14c] that if this crystalline sample is simply ground by hand in a mortar and pestle or a less crystalline sample prepared by rapid crystallization, then the Mössbauer characteristics are different. For these samples two doublets are seen in each spectrum in the temperature region where this complex converts from low to high spin. The explanation for this sample history dependence focused on variable amounts of defect structure. It was suggested that grinding the sample or crystallizing it rapidly gave a sample with a greater level of defect concentration than is present in a well-crystallized sample. The increased defect concentration would be expected to impact on the kinetics associated with phase transitions. In the nucleation and growth mechanism[32] for phase transitions the conversion of a crystallite from one phase to another is affected by at least two rates. The rate of formation of a critical size nucleus of the minority phase in the majority phase is important. Also, the rate at which critical-size nuclei grow to become large regions (domain wall movement) is important. The concentration of defects impacts on both of these rates. It appears that, relative to the samples prepared by the small scale preparation (method I), the heat-capacity samples prepared on large scale (method II) have a somewhat greater defect concentration.

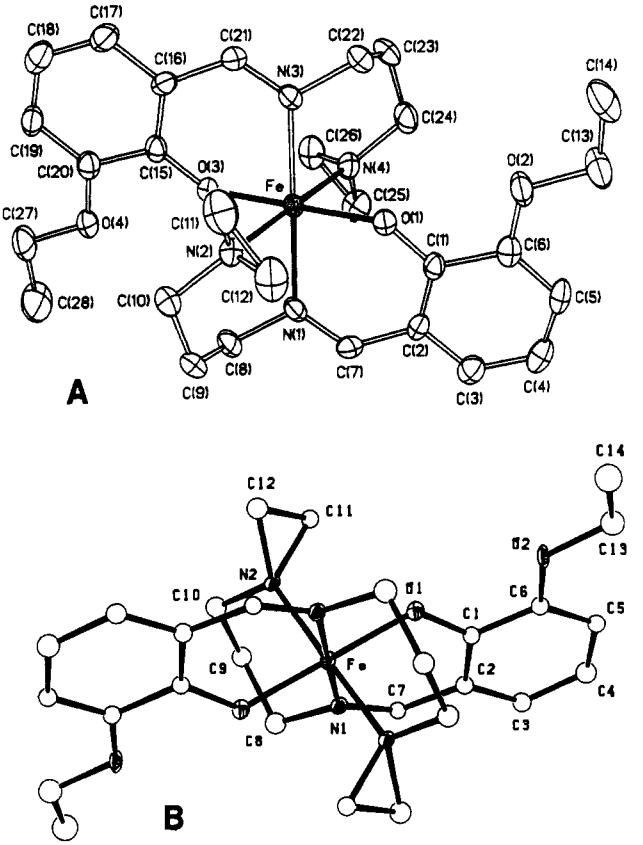

Figure 6. ORTEP plot of the Fe^{III} cation in $[Fe(3\text{-}OEt\text{-}SalAPA)_2](ClO_4)\cdot C_6H_5Cl$. In part A is shown the cation in the 296 K structure, whereas in part B only one of the two crystallographically different Fe^{III} cations in the 158 K structure is shown.

X-ray Structures of $[Fe(3\text{-}OEt\text{-}SalAPA)_2](ClO_4)\cdot S$, Where S is C_6H_5Cl, C_6H_5Br, or $o\text{-}C_6H_4Cl_2$. The single-crystal X-ray structure of the benzene solvate in this series has been determined[23] at 20, 128, 175, 298, and 300 K. At 298 and 300 K this complex crystallizes as $C2/c$ ($Z = 4$), whereas in the 20–175 K range it is of $P2_1/c$ ($Z = 4$) symmetry. The nonsolvated $[Fe(3\text{-}OEt\text{-}SalAPA)_2]ClO_4$ complex was found in this study to be isostructural at room temperature with $[Fe(3\text{-}OMe\text{-}SalAPA)_2]ClO_4$, for which the structure has been reported[24] to be $P\bar{1}$ at 286 K.

In this study the single-crystal structure of the C_6H_5Cl solvate was determined at 158 and 296 K (Figure 6), that of the C_6H_5Br solvate was determined at 163 and 296 K, and the structure of the $o\text{-}C_6H_4Cl_2$ solvate was determined at 298 K. Tables of selected bond lengths and angles for all five of these structure determinations are available in the supplementary material. The $o\text{-}C_6H_4Cl_2$ solvate is isostructural with the C_6H_6 solvate at 298 K. The C_6H_5Cl and C_6H_5Br solvates qualitatively seem to behave similarly. At 296 K both of these solvates crystallize in the $P2_1/c$ space group. However, this is *not* the same phase as the lowest

(29) (a) Maeda, Y.; Takashima, Y.; Matsumoto, N.; Okyoshi, A. *J. Chem. Soc., Dalton Trans.* **1986**, 115–1123. (b) Maeda, Y.; Tsutsumi, N.; Takashima, Y. *Inorg. Chem.* **1984**, *23*, 2440–2447. (c) Maeda, Y.; Ohshio, H.; Takashima, Y. *Chem. Lett.* **1982**, 943–946. (d) Maeda, Y.; Oshio, H.; Takashima, Y.; Mikuriya, M.; Hidaka, M. *Inorg. Chem.* **1985**, *25*, 2958–2962.

(30) Wikman, H. H. *Mössbauer Effect Methodology*; Gruverman, I. J., Ed.; Plenum Press: New York, 1966, Vol. 2, p 39.

(31) Herber, R. H. *Inorg. Chem.* **1987**, *26*, 173.

(32) Rao, C. N. R.; Rao, K. H. *Phase Transitions in Solids*; McGraw-Hill: New York, 1978.

Table XI. Iron–Ligand Bond Lengths (Å) for $[Fe(3\text{-}OEt\text{-}SalAPA)_2](ClO_4)_2 \cdot S$ Where S Is C_6H_6, C_6H_5Cl, C_6H_5Br, or $o\text{-}C_6H_4Cl_2$[a]

		S = C_6H_6		S = C_6H_5Cl		S = C_6H_5Br		
		128 K	300 K	158 K	296 K	163 K	296 K	S = $o\text{-}C_6H_4Cl_2$ 296 K
cation I[b]	Fe–N(amine)	2.028(5)	2.176(3)	2.040(6)	2.185(6)	2.115(7)	2.179(9)	2.198(6)
	Fe–N(imine)	1.958(5)	2.085(3)	1.968(6)	2.095(6)	2.027(8)	2.091(11)	2.081(4)
	Fe–O	1.852(4)	1.921(2)	1.860(5)	1.914(6)	1.900(7)	1.917(10)	1.925(3)
cation II[b]	Fe–N(amine)	2.032(5)		2.046(6)		2.060(7)		
	Fe–N(imine)	1.961(5)		1.969(6)		1.974(7)		
	Fe–O	1.850(4)		1.866(5)		1.882(7)		

[a] Average bond lengths are given if the cation is not on a center of inversion. [b] Roman numerals indicate each type of crystallographically unique cation.

Table XII. Chelate Bite Angles (deg) for $[Fe(3\text{-}OEt\text{-}SalAPA)_2](ClO_4) \cdot S$ Where S is C_6H_6, C_6H_5Cl, C_6H_5Br, or $o\text{-}C_6H_4Cl_2$[a]

		S = C_6H_6		S = C_6H_5Cl		S = C_6H_5Br		
		128 K	300 K	158 K	296 K	163 K	296 K	S = $o\text{-}C_6H_4Cl_2$ 296 K
cation I[b]	N(amine)–Fe–N(imine)	85.0(2)	83.0(1)	85.2	82.9	83.8	81.9	82.9
	N(amine)–Fe–O	91.7(2)	92.7(1)	92.7	93.0	92.4	93.1	93.6
	N(imine)–Fe–O	90.5(2)	87.2(1)	91.2	87.3	89.2	89.2	87.4
cation II[b]	N(amine)–Fe–N(imine)	88.1(2)		85.1		84.6		
	N(amine)–Fe–O	95.2(2)		92.0		91.7		
	N(imine)–Fe–O	90.6(2)		90.2		90.5		

[a] Average bond lengths are given if the cation is not on a center of inversion. [b] Roman numerals indicate each type of crystallographically unique cation.

temperature $P2_1/c$ phase of the benzene solvate. The asymmetric unit in the 298 K $P2_1/c$ phase of the C_6H_5Cl solvate has only one Fe^{III} cation, whereas, the $P2_1/c$ phase of the C_6H_6 solvate has two different Fe^{III} cations in the asymmetric unit. Finally, the C_6H_5Cl and C_6H_5Br solvates both convert relatively abruptly from $P2_1/c$ to $P2_1/a$ as the temperature is decreased. It must be emphasized that the $P2_1/a$ setting is *not* just a reformulation of the $P2_1/c$ setting.

The arrangement of the two tridentate ligands is the same for the $[Fe(3\text{-}OEt\text{-}SalAPA)_2]^+$ cations in all five solvates as well as the nonsolvated complex. The two 3-OEt-SalAPA$^-$ tridentate ligands are bonded to the Fe^{III} ion in a completely *trans* ligand atom configuration. In Figure 6 are shown ORTEP plots of the Fe^{III} cation in the C_6H_5Cl solvate as determined at 158 and 296 K. The two O ligand atoms are trans to each other, as are the two N(amine) ligand atoms and the two tridentate N(imine) atoms. Apparently this configuration of the two tridentate ligands is stabilized in part by the propylene linkages between the imine and amine nitrogen atoms. In several other bis(tridentate) Fe^{III} spin-crossover complexes for which there are X-ray structures the two tridentate ligands coordinate meridionally with only the two imine nitrogen atoms trans. This is the case for $[Fe(acpa)_2]X$,[29d] where Hacpa is *N*-(1-acetyl-2-propylidene)(2-pyridylomethyl)amine and X$^-$ is either PF_6^- or BPh_4^-, as well as for $[Fe(X\text{-}Salmeen)_2]PF_6$[33] where X-Salmeen$^-$ is a substituted version of the ligand resultant from a Schiff base condensation of salicylaldehyde and *N*-methylethylenediamine and several other[3,34] Fe^{III} spin-crossover complexes. The only other spin-crossover Fe^{III} complexes which exhibit an all trans configuration (same types of ligand atoms trans to each other) are found for complexes with hexadentate ligands: $[FeL]NO_3$,[35] where L is Sal_2-3,3,3-tet or Sal_2-3,2,3-tet.

For the C_6H_6, C_6H_5Cl, and C_6H_5Br solvates where X-ray structures are available both at room and at low temperatures a common observation is made. In the low-temperature structure for each of these three complexes there are two crystallographically different Fe^{III} cations. At room temperature there is only one crystallographically distinct Fe^{III} cation for each of these three solvates. The $o\text{-}C_6H_4Cl_2$ solvate also only has one Fe^{III} cation at 298 K. On the other hand, the nonsolvated complex $[Fe(3\text{-}OMe\text{-}SalAPA)_2](ClO_4)$, which is isostructural to the 3-OEt substituted analog, has been reported[24] to have two crystallographically different cations at 295 K. From the average Fe–N(amine) bond lengths in this nonsolvated complex it was concluded that cation A is 28% high spin, whereas cation B at 295 K is 85% high spin. These values agree with the magnetic susceptibility results for this same 3-OMe-substituted complex, which is found to be ~56% high spin at 290 K. At room temperature the C_6H_5Cl, C_6H_5Br, and $o\text{-}C_6H_4Cl_2$ solvates are all high spin (see Figure 1) and the C_6H_6 solvate is near to being all high spin. The 128 K structure reported[23] for the C_6H_6 solvate is at a temperature where this solvate is essentially all low spin. The temperatures of the low-temperature X-ray structures of the C_6H_5Cl (158 K) and C_6H_5Br (163 K) solvates are such that there is some amount of high-spin complexes present (see Figure 1).

Since the benzene solvate has been structurally characterized in both its low- and high-spin state, it can be used as a gauge of changes in bond lengths. In Table XI are given the iron–ligand atom bond distances for all the structurally characterized complexes. For Fe^{III} cations which are not sitting on a crystallographic center of inversion, average values of Fe–N(amine), Fe–N(imine), and Fe–O bond lengths are given. In the case of the C_6H_6 solvate the Fe–N(amine) distance decreases from 2.176(3) Å at 300 K to 2.028(5) Å at 128 K; the Fe–N(imine) distance decreases from 2.085(3) Å at 300 K to 1.958(5) Å at 128 K; the Fe–O distance decreases from 1.921(2) Å at 300 K to 1.852(4) Å at 128 K. Clearly the Fe–N bond lengths change more than the Fe–O lengths. From the bond lengths in Table XII it can be seen that at 163 K the two different cations in the C_6H_5Br solvate are dimensionally different. From the bond length changes seen for the benzene solvate it can be estimated that one cation is ~20% high spin and the other is ~60% high spin for the C_6H_5Br solvate at 163 K (see Figure 1). The average is ~40%, which is somewhat higher than is estimated from the susceptibility data for 163 K. However, the crystal temperature determination for the X-ray structural work is probably not nearly as accurate as that employed in the SQUID susceptometer. Regardless of the details it is clear that the two crystallographically distinct cations in the 163 K C_6H_5Br structure are dimensionally different. This

(33) Sim, P. G.; Sinn, E.; Petty, R. H.; Merrill, C. L.; Wilson, L. J. *Inorg. Chem.* **1981**, *30*, 1213.
(34) Sinn, E.; Sim, G.; Dose, E. V.; Tweedle, M. F.; Wilson, L. J. *J. Am. Chem. Soc.* **1978**, *100*, 3375.
(35) Ito, T.; Sugimoto, M.; Ito, H.; Toriumi, K.; Nakayama, H.; Mori, J. W.; Sekizaki, M. *Chem. Lett.* **1983**, 121.

Table XIII. Average θ Values, Ranges of θ Values, and Standard Deviations for $[Fe(3\text{-OEt-SalAPA})_2](ClO_4)\cdot S$ Where S Is C_6H_6, C_6H_5Cl, C_6H_5Br, or $o\text{-}C_6H_4Cl_2$

		S = C_6H_6		S = C_6H_5Cl		S = C_6H_5Br		S = $o\text{-}C_6H_4Cl_2$
		128 K	300 K	158 K	296 K	163 K	296 K	296 K
cation I[a]	θ_{ave}, deg	60.0	60.0	60.0	60.0	60.0	60.0	60.0
	θ_{range}, deg	58.0–61.3	56.1–63.4	57.8–61.3	55.4–63.6	57.0–62.0	55.4–63.3	51.1–65.8
	θ_{ϕ}, deg	1.4	3.0	1.6	3.0	2.2	2.9	6.4
cation II[a]	θ_{ave}, deg	60.0		60.0		60.0		
	θ_{range}, deg	54.4–63.0		85.7–61.3		54.5–62.9		
	θ_{ϕ}, deg	3.9		1.6		3.9		

[a] Roman numerals indicate each type of crystallographically unique cation.

is interesting for the two crystallographically distinct cations in the 158 K C_6H_5Cl solvate structure are dimensionally quite similar.

A comparison of the iron–chelate bite angles is made in Table XII. For an octahedral complex each of the bite angles equals 90°. It is seen that the range of bite angles is greatest for the high-temperature structures and that the distortions from octahedral symmetry among the high-temperature structures are of the same magnitude from one solvate to another. Direct comparison of the structural parameters of the low-temperature structures is made difficult due to the fact that the solvate complexes are comprised of different fractions of high- and low-spin species at the temperatures given. The 128 K benzene structure, however, is almost all low spin and it exhibits the smallest deviation from octahedral symmetry. These bite angles ranges are smaller than those observed for the cation in $[Fe(acac)_2trien]PF_6$[36] (high spin) with a range of 76.7 to 102.1° or for the cation in $[Fe(3\text{-OMe-Salmeen})_2]PF_6$[3,23] where the low-spin cation has a bite angle range from 83.3 to 95.6°. The chelate rings are six-membered rings for the 3-OEt-SalAPA$^-$ complexes. Other N_4O_2 ferric spin-crossover complexes have their tridentate ligands coordinated meridionally with five- and six-membered chelate rings. This explains why the $[Fe(3\text{-OEt-SalAPA})_2]^+$ cations are less distorted in their chelate ring bites compared to other N_4O_2 ferric complexes.

Concluding Comments

Data have been presented for the $[Fe(3\text{-OEt-SalAPA})_2](ClO_4)\cdot S$ series of spin-crossover complexes. The spin-crossover transformation was found to be most gradual (*i.e.*, largest temperature range) for the nonsolvated complex where S is absent. Addition of a solvate molecule S to the lattice leads to a considerably more abrupt transformation. The C_6H_5Cl solvate exhibits the most abrupt spin-crossover transformation.

All of the complexes in the series give EPR spectra which at intermediate temperatures simultaneously show signals from both low- and high-spin complexes. The spin-state interconversion rates are slower than the EPR time scale ($<\sim 10^9$–10^{10} s^{-1}). Mössbauer spectra for the complexes give time scale assessments which are sample-history dependent. Polycrystalline samples made in a small ($\leq$1 g) scale preparation show a single average Mössbauer doublet at all temperatures, indicating a fast spin-state interconversion rate. On the other the large (17–20 g) scale polycrystalline complexes show spectra at intermediate temperatures which are comprised of two doublets, one for the low-spin and the other for the high-spin complexes. It is suggested that different levels of defect concentration are present in the two types of samples. The apparently slower rate of spin-state interconversion for the large-scale preparation sample is a reflection of slow kinetics associated with domain wall movement in phase transitions.

At least five structurally different phases are present for the six complexes in the $[Fe(3\text{-OEt-SalAPA})_2](ClO_4)\cdot S$ series. The nonsolvated complex is $P\bar{1}$ at room temperature. The benzene solvate converts from $C2/c$ at room temperature to $P2_1/c$ at temperatures below 175 K. The $o\text{-}C_6H_4Cl_2$ solvate is isostructural to the benzene solvate at room temperature. The C_6H_5Cl and C_6H_5Br solvates convert from $P2_1/c$ at room temperature to $P2_1/a$ at low temperature; furthermore, their $P2_1/c$ phase is different than the low-temperature benzene $P2_1/c$ phase.

In the following paper an attempt will be made to delineate the structural, thermodynamic, and dynamical characteristics which distinguish these different phases.

Acknowledgment. We are grateful for funding from National Institutes of Health Grant HL13652 (D.N.H.) and National Science Foundation Grant CHE-9115286 (D.N.H.).

Supplementary Material Available: Tables of magnetic susceptibility data for all six complexes, tables of bond lengths and angles, hydrogen atom parameters, and thermal parameters for the C_6H_5Cl (158 and 296 K), C_6H_5Br (163 and 296 K) and $o\text{-}C_6H_4Cl_2$ (298 K) solvates, tables of analytical data for five of the solvates, tables of Mössbauer parameters for two of the solvates, and figure showing Mössbauer spectra of the C_6H_5Br and $o\text{-}C_6H_4Cl_2$ solvates and a figure showing X-ray diffraction patterns for five of the solvates (40 pages). Ordering information is given on any current masthead page.

(36) Sinn, E.; Sim, G.; Dose, E. V.; Tweedle, M. F.; Wilson, L. J. *J. Am. Chem. Soc.* **1978**, *100*, 3375.